

In-plane spin excitation anisotropy in the paramagnetic state of NaFeAsYu Song,^{1,2} Louis-Pierre Regnault,³ Chenglin Zhang,^{1,2} Guotai Tan,² Scott V. Carr,^{1,2} Songxue Chi,⁴ A. D. Christianson,⁴ Tao Xiang,⁵ and Pengcheng Dai^{1,2,5,*}¹*Department of Physics and Astronomy, Rice University, Houston, Texas 77005, USA*²*Department of Physics and Astronomy, The University of Tennessee, Knoxville, Tennessee 37996-1200, USA*³*SPSMS-MDN, UMR-E CEA/UJF-Grenoble 1, INAC, Grenoble, F-38054, France*⁴*Quantum Condensed Matter Division, Oak Ridge National Laboratory, Oak Ridge, Tennessee 37831, USA*⁵*Beijing National Laboratory for Condensed Matter Physics, Institute of Physics, Chinese Academy of Sciences, Beijing 100190, China*

(Received 22 May 2013; revised manuscript received 2 October 2013; published 17 October 2013)

We use unpolarized and polarized inelastic neutron scattering to study low-energy spin excitations in NaFeAs, which exhibits a tetragonal-to-orthorhombic lattice distortion at $T_s \approx 58$ K followed by a collinear antiferromagnetic (AF) order below $T_N \approx 45$ K. In the AF ordered state ($T < T_N$), spin waves are entirely c -axis polarized below ~ 10 meV, exhibiting a gap of ~ 4 meV at the AF zone center and disperse to ~ 7 meV near the c -axis AF zone boundary. On warming to the paramagnetic state with orthorhombic lattice distortion ($T_N < T < T_s$), spin excitations become anisotropic within the FeAs plane. Upon further warming to the paramagnetic tetragonal state ($T > T_s$), spin excitations become more isotropic. Since similar magnetic anisotropy is also observed in the paramagnetic tetragonal phase of superconducting BaFe_{1.904}Ni_{0.096}As₂, our results suggest that the spin excitation anisotropy in superconducting iron pnictides originates from similar anisotropy already present in their parent compounds.

DOI: [10.1103/PhysRevB.88.134512](https://doi.org/10.1103/PhysRevB.88.134512)

PACS number(s): 74.70.Xa, 75.30.Gw, 78.70.Nx

I. INTRODUCTION

The parent compounds of iron pnictide superconductors are semimetallic antiferromagnets exhibiting a tetragonal to orthorhombic lattice distortion at temperature T_s followed by a paramagnetic to antiferromagnetic (AF) phase transition at T_N .¹⁻⁸ The magnetic structure is collinear with the ordered moment aligned antiferromagnetically along the a axis of the orthorhombic lattice [Fig. 1(a)]. From transport,⁹ resonant ultrasound,¹⁰ angle-resolved photoemission spectroscopy (ARPES),¹¹⁻¹³ inelastic neutron scattering,¹⁴ magnetic torque,¹⁵ and scanning tunneling microscopy (STM)¹⁶⁻¹⁸ measurements, it is clear that iron pnictides have electronic anisotropy above T_N implying an underlying electronic nematic phase.¹⁹ However, the microscopic origin of the observed electronic anisotropy is still an issue of debate. In both the strong and weak coupling limits, the electronic anisotropy could be caused by a spin nematic phase (spin anisotropy) in the paramagnetic orthorhombic phase above T_N but below T_s .^{20,21} Alternatively, orbital ordering in the paramagnetic orthorhombic state may also induce the observed electronic anisotropy.²²⁻²⁶ Although transport²⁷ and x-ray diffraction²⁸ experiments in magnetic fields on electron-doped BaFe_{2-x}Co_xAs₂ reveal clear evidence for anisotropic in-plane static spin susceptibility ($\chi_a \neq \chi_b$) in the paramagnetic orthorhombic state ($T_N \leq T \leq T_s$), it is still unclear if such in-plane susceptibility anisotropy is field induced or intrinsic to these materials at zero field. Furthermore, recent STM¹⁷ and transport measurements^{29,30} suggest that the resistivity anisotropy in Co-doped BaFe₂As₂ arises from Co-impurity scattering, and is not an intrinsic property of these materials.

In this article, we use unpolarized and polarized neutron scattering to study spin waves and paramagnetic spin excitations in NaFeAs.⁶ In contrast to BaFe₂As₂, where the orthorhombic lattice distortion (T_s) and AF order (T_N) occur at similar temperatures,^{3,4} NaFeAs has clearly separated

structural and magnetic phase transitions at $T_s \approx 58$ K and $T_N \approx 45$ K, respectively.^{6,7} Below the AF ordering temperature, the iron spins in NaFeAs order antiferromagnetically along the a axis of the orthorhombic structure and ferromagnetically along the b axis.^{6,7} In the low-temperature AF ordered state, NaFeAs forms randomly distributed orthorhombic twin domains rotated 90° apart similar to BaFe₂As₂.¹⁴ Low-energy spin excitations in iron pnictides are centered around the AF ordering wave vectors $\mathbf{Q}_{AF} = (\pm 1, 0)$ and $(0, \pm 1)$ corresponding to the two sets of domains, thus allowing spin excitations polarized along different crystallographic axes to be determined in a twinned sample.³¹⁻³⁵ In the AF ordered state ($T < T_N$) of NaFeAs, our unpolarized neutron scattering measurements find that spin waves are gapped below ~ 4 meV at the AF zone center and disperse to ~ 7 meV near the c -axis AF zone boundary. Similar to BaFe₂As₂,³² neutron polarization analysis indicates that spin waves in NaFeAs are entirely c -axis polarized for energies below ~ 10 meV. On warming the system to the paramagnetic orthorhombic state above T_N , the c -axis polarized spin waves become anisotropic paramagnetic scattering. By carefully measuring wave vector dependence of the paramagnetic scattering, we show that the magnetic response M (M is related to the imaginary part of the dynamic susceptibility $\chi''(\mathbf{Q}, E)$ via the Bose factor $M = \chi''(\mathbf{Q}, E)/[1 - \exp(-E/k_B T)]$) at the AF wave vector and $E = 6$ meV has in-plane anisotropy with $M_a \geq M_b$ in the paramagnetic orthorhombic state ($T_N \leq T \leq T_s$) of NaFeAs. Such anisotropy becomes much weaker above T_s and spin excitations become nearly isotropic. Since the in-plane anisotropic paramagnetic spin excitations in NaFeAs are similar to those observed in the tetragonal phase of superconducting BaFe_{1.906}Ni_{0.096}As₂,³⁵ the spin excitation anisotropy in superconducting iron pnictides originates from similar anisotropy already present in the parent compound. While these results suggest the presence of a spin nematic state

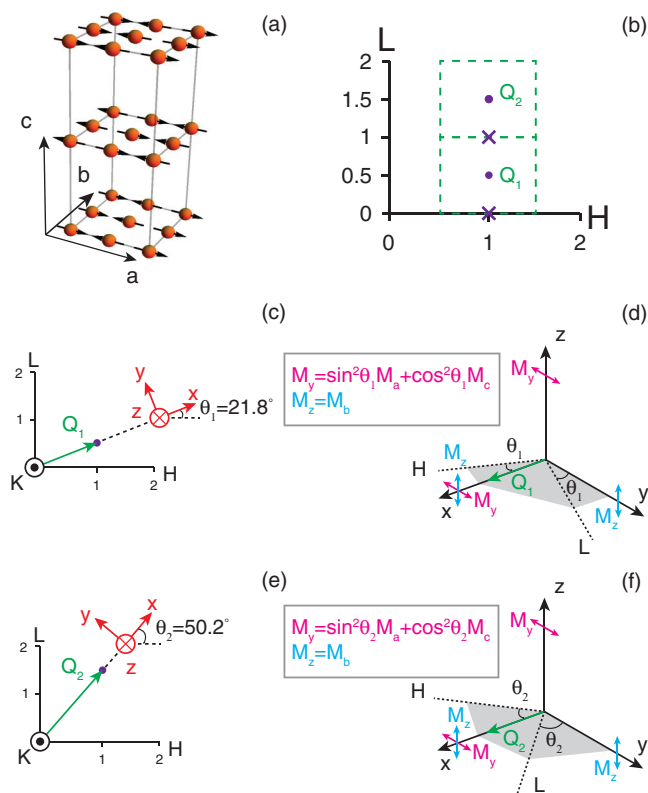


FIG. 1. (Color online) (a) The orthorhombic chemical unit cell of NaFeAs (enclosed by gray lines, two orthorhombic chemical unit cells are stacked along the c axis). The black arrows indicate directions of the ordered moments and orange spheres represent Fe atoms, Na and As atoms are not shown. (b) Points in reciprocal space probed in this work. The points represent magnetic zones centers ($L = 0.5, 1.5$) while the crosses represent magnetic zone boundaries ($L = 0, 1$) along the $(1, 0, L)$ direction. The dashed green lines enclose the magnetic Brillouin zone. The relationship between the neutron polarization directions (x, y, z) and the scattering plane are shown in (c) for $\mathbf{Q} = (1, 0, 0.5)$ and in (e) for $(1, 0, 1.5)$. The angle between x direction and the H axis is denoted as θ_1 for $(1, 0, 0.5)$ and θ_2 for $(1, 0, 1.5)$. The magnetic components measured in each channel and their relationships to the magnetic components projected onto the crystal axes are shown in (d) for $\mathbf{Q} = (1, 0, 0.5)$ and in (f) for $(1, 0, 1.5)$. Only SF channels are measured in this work. σ_x^{SF} contains both M_y and M_z magnetic components, whereas only M_y and M_z contribute to σ_z^{SF} and σ_y^{SF} , respectively. The relationships between the magnetic components along the neutron polarization directions (M_x, M_y , and M_z) and crystal axes (M_a, M_b , and M_c) are shown in the boxes in (d) and (f) for $L = 0.5$ and $L = 1.5$, respectively.

in the paramagnetic orthorhombic phase of NaFeAs, they may also be consistent with anisotropic critical fluctuations due to a single-ion anisotropy in the orthorhombic phase.³⁶

II. EXPERIMENTAL RESULTS

Figure 1(a) shows the collinear AF structure of NaFeAs with orthorhombic lattice parameters $a = 5.589$, $b = 5.569$, and $c = 6.991$ Å.⁶ We define momentum transfer \mathbf{Q} in three-dimensional reciprocal space in Å⁻¹ as $\mathbf{Q} = H\mathbf{a}^* + K\mathbf{b}^* + L\mathbf{c}^*$, where H, K , and L are Miller indices and $\mathbf{a}^* = \hat{\mathbf{a}}2\pi/a$, $\mathbf{b}^* = \hat{\mathbf{b}}2\pi/b$, $\mathbf{c}^* = \hat{\mathbf{c}}2\pi/c$. About 5 g of single

crystals of NaFeAs were coaligned in the $[H, 0, L]$ scattering plane [Fig. 1(b)]. In this notation, the AF Bragg peaks and zone centers occur at $[1, 0, L]$ with $L = 0.5, 1.5, \dots$, while the AF zone boundaries along the c axis occur at $L = 0, 1, 2, \dots$.⁶ Our polarized neutron scattering experiments were carried out using the IN22 thermal triple-axis spectrometer at the Institut Laue-Langevin, Grenoble, France.³¹ Consistent with previous notation,³¹ we define the neutron polarization directions along \mathbf{Q} as x , perpendicular to \mathbf{Q} but in the scattering plane as y , and perpendicular to \mathbf{Q} and the scattering plane as z , respectively [Figs. 1(c) and 1(e)]. Since neutron scattering is only sensitive to magnetic scattering components perpendicular to the momentum transfer \mathbf{Q} , one can probe magnetic responses within the y - z plane (M_y and M_z) [Fig. 1(c)].

Within the scattering plane, the measured magnetic response at \mathbf{Q} give $M_y = \sin^2 \theta M_a + \cos^2 \theta M_c$ and $M_z = M_b$, where the angle between \mathbf{Q} and $[H, 0, 0]$ is θ , and M_a, M_b , and M_c are spin excitation intensities along the orthorhombic a -, b -, and c -axis directions, respectively.³¹ This is related to the observed neutron spin-flip (SF) scattering cross sections for different neutron polarization directions σ_x^{SF} , σ_y^{SF} , and σ_z^{SF} via

$$\begin{aligned} \sigma_x^{\text{SF}} &= \frac{R}{R+1}(\sin^2 \theta M_a + \cos^2 \theta M_c) + \frac{R}{R+1} M_b + B, \\ \sigma_y^{\text{SF}} &= \frac{1}{R+1}(\sin^2 \theta M_a + \cos^2 \theta M_c) + \frac{R}{R+1} M_b + B, \\ \sigma_z^{\text{SF}} &= \frac{R}{R+1}(\sin^2 \theta M_a + \cos^2 \theta M_c) + \frac{1}{R+1} M_b + B, \end{aligned} \quad (1)$$

where R is the flipping ratio for non-spin-flip (NSF) and SF scattering ($R = \sigma_{\text{Bragg}}^{\text{NSF}} / \sigma_{\text{Bragg}}^{\text{SF}} \approx 15$) and B is the background scattering that may be larger than the magnetic scattering. Therefore, to conclusively determine the magnetic anisotropy along the three crystallographic directions M_a, M_b , and M_c of the orthorhombic lattice, we need to measure neutron SF scattering at two or more equivalent AF wave vectors with different angle θ between the wave vector \mathbf{Q} and $[H, 0, 0]$.³⁵ To compare the estimated M_a, M_b , and M_c at different wave vectors, we need to consider in addition the differences in the magnetic form factor $F(\mathbf{Q})$ and instrumental resolution r . For example, at the AF zone center $[1, 0, L]$ ($L = 0.5, 1.5, \dots$) positions, by combining the cross sections measured at $\mathbf{Q} = (1, 0, 0.5)$ and $\mathbf{Q} = (1, 0, 1.5)$ for a particular energy transfer (σ_x^{SF} , σ_y^{SF} , and σ_z^{SF} at both wave vectors), we have five quantities (M_a, M_b, M_c , and B at the two wave vectors) to be determined from up to six cross sections [Figs. 1(c)–1(f)]. We either measured all six cross sections and used the overdetermination to improve estimates of M_a, M_b , and M_c [Figs. 3(a)–3(d)] or measured five cross sections which uniquely determines the magnetic response [Figs. 4(c) and 4(d)]. A similar procedure is used to analyze data for the zone boundary along the c axis ($L = 0, 1$).

In previous unpolarized neutron scattering measurements of spin waves in Na_{0.9}FeAs, the onset of spin gap at the AF zone center $\mathbf{Q} = (1, 0, 1.5)$ is observed at approximately ~ 10 meV.³⁷ Figure 2 summarizes our unpolarized neutron measurements on NaFeAs using HB-3 triple-axis spectrometer at the High-Flux-Isotope Reactor (HFIR), Oak Ridge National Laboratory. The monochromator, analyzer, and filters are all pyrolytic graphite. The collimations are

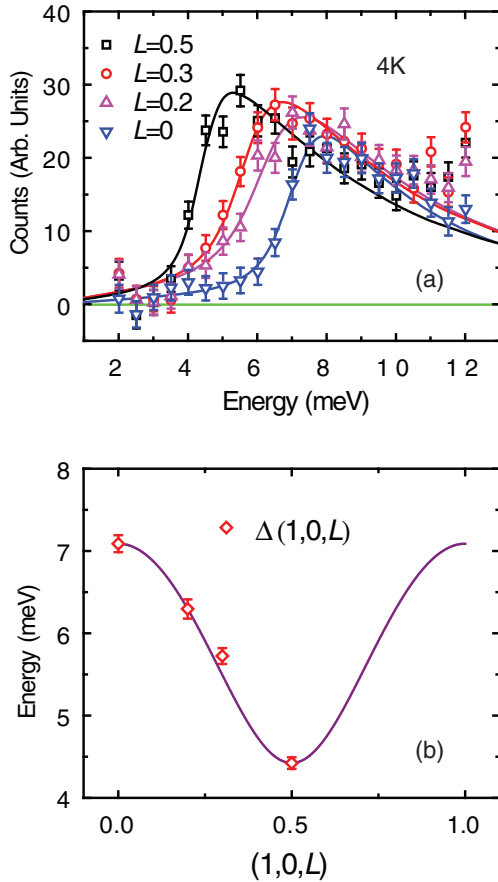


FIG. 2. (Color online) (a) Constant- \mathbf{Q} scans at $(1,0,L)$ at 4 K for $L = 0, 0.2, 0.3,$ and 0.5 with unpolarized neutrons after background has been subtracted. Solid lines are fits to the response of a damped harmonic oscillator convolved with instrumental resolution with low-energy spin waves modeled as $E(\mathbf{Q}) = \sqrt{\Delta(1,0,L)^2 + v_a^2 h^2 + v_b^2 k^2}$, where $(h,k) = (H,K) - (1,0)$.³⁸ Data points with $E < 11$ meV are used in the fits. (b) Dispersion of the low-energy spin waves along the $(1,0,L)$ direction, points are fitted gap values $\Delta(1,0,L)$, the purple solid line is the dispersion from linear spin wave theory using effective exchange couplings from Ref. 39.

48'-40'-sample-40'-120' with the final neutron energy fixed at $E_f = 14.68$ meV. Our energy scan at the AF zone center wave vectors $\mathbf{Q} = (1,0,0.5)$ reveals a clear spin gap of ~ 4 meV [Fig. 2(a)], much smaller than that of $\text{Na}_{0.9}\text{FeAs}$.³⁷ Upon moving the wave vectors to $\mathbf{Q} = (1,0,0.3), (1,0,0.2),$ and $(1,0,0)$, the spin gap changes to ~ 7 meV at the c -axis AF zone boundary position with $L = 0$ [Fig. 2(a)]. To understand these data, we fit the spin wave spectra with a damped harmonic oscillator $\chi''(\mathbf{Q}, E) = AE_0(\mathbf{Q})\Gamma E / \{(\Gamma E)^2 + [E_0^2(\mathbf{Q}) - E^2]^2\}$, convolved with instrumental resolution similar to previous work.³⁸ The spin wave dispersion is $E(\mathbf{Q}) = \sqrt{\Delta(1,0,L)^2 + v_a^2 h^2 + v_b^2 k^2}$, where $\Delta(1,0,L)$ is the spin gap value, and v_a and v_b are spin wave velocities along the a and b axes, respectively. The solid lines in Fig. 2(a) show the fits using spin wave velocities of NaFeAs obtained from high-energy time-of-flight measurements.³⁹ Figure 2(b) shows the c -axis dispersion of the spin waves. Given the almost identical T_N and T_s between

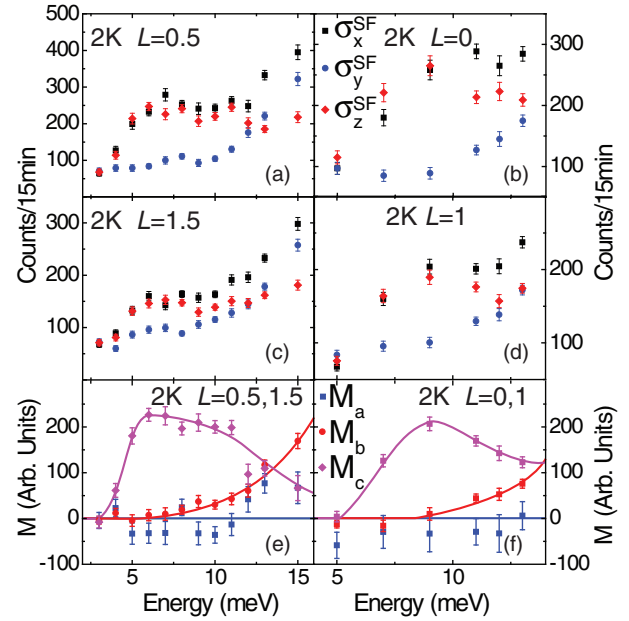


FIG. 3. (Color online) Constant- \mathbf{Q} scans in the AF ordered state ($T = 2$ K) at $\mathbf{Q} = (1,0,L)$ with $L = 0, 0.5, 1,$ and 1.5 are shown in (b), (a), (d), and (c), respectively. All three spin-flip channels are measured, denoted as $\sigma_x^{\text{SF}}, \sigma_y^{\text{SF}},$ and σ_z^{SF} for the three different neutron polarization directions. From the measured cross sections at $(1,0,0.5)$ and $(1,0,1.5)$, the magnetic components at the magnetic zone center along the crystallographic axes $M_a, M_b,$ and M_c are determined and plotted in (e). Similarly, (f) shows the magnetic components along different crystallographic axes for magnetic zone boundaries at $\mathbf{Q} = (1,0,0)$ and $(1,0,1)$. The solid lines in (e) and (f) are guides to the eye.

our NaFeAs samples⁷ and $\text{Na}_{0.9}\text{FeAs}$,³⁷ it is unclear why their spin gap values are so different.

Figure 3 shows the energy scans at the AF zone center $\mathbf{Q} = (1,0,0.5), (1,0,1.5)$ and zone boundary $(1,0,0), (1,0,1)$ with different neutron polarizations in the low-temperature AF ordered state. At the AF wave vectors $\mathbf{Q} = (1,0,0.5)$ [Fig. 3(a)], we find a clear spin gap of ~ 4 meV consistent with unpolarized data of Fig. 2. Furthermore, σ_x^{SF} are similar to σ_z^{SF} for $E \leq 11$ meV while $\sigma_x^{\text{SF}} > \sigma_y^{\text{SF}} > \sigma_z^{\text{SF}}$ for $E > 11$ meV. Similar results are obtained at $\mathbf{Q} = (1,0,1.5)$ [Fig. 3(c)]. In order to obtain $M_a, M_b,$ and M_c , we assume Fe^{2+} magnetic form factor and correct for the instrumental resolution factor r at these two wave vectors. The obtained $M_a, M_b,$ and M_c are shown in Fig. 3(e). We see that spin waves in NaFeAs are transverse to the ordered moment direction and almost entirely c -axis polarized with $M_a \approx M_b \approx 0$ for $E \leq 10$ meV [Fig. 1(e)]. This is similar to the low temperature spin waves in BaFe_2As_2 .³² For spin wave energies above 10 meV, we see a dramatic reduction in M_c and a corresponding increase in M_b . Most surprisingly, there appears to be a small but nonzero M_a around 12 meV, suggesting the possible presence of longitudinal spin excitations. This is disallowed for spin waves in a classical local moment Heisenberg Hamiltonian, but may be present in NaFeAs due to itinerant electrons.⁸ Figures 3(b) and 3(d) show similar results at the AF zone boundary $\mathbf{Q} = (1,0,0)$ and $(1,0,1)$. The energy dependence of $M_a, M_b,$ and M_c are shown in Fig. 3(f). Again, spin waves

are entirely polarized along the c axis for energies below 10 meV and have no longitudinal component for the probed energy range. We note that recent polarized neutron scattering experiments on BaFe_2As_2 have conclusively established the presence of longitudinal spin-wave excitations in the AF ordered phase.⁴⁰

Figures 4(a) and 4(b) plot the energy scans in the paramagnetic tetragonal state ($T = 60$ K) at the AF wave vectors $\mathbf{Q} = (1,0,0.5)$ and $(1,0,1.5)$, respectively. From Eq. (1) we note that isotropic paramagnetic scattering should imply $\sigma_x^{\text{SF}}/2 \approx \sigma_y^{\text{SF}} \approx \sigma_z^{\text{SF}}$ in the limit of large R and negligible background scattering ($B \rightarrow 0$). This is clearly not the case in Figs. 4(a) and 4(b), thus suggesting the presence of finite background scattering. In this case, one can estimate the magnetic anisotropy using $\sigma_z^{\text{SF}} - \sigma_y^{\text{SF}} = (\sin^2 \theta M_a + \cos^2 \theta M_c - M_b)(R - 1)/(R + 1) \propto M_y - M_z$ to eliminate the influence of background. Since data in Figs. 4(a) and 4(b) suggest $\sigma_x^{\text{SF}} > \sigma_y^{\text{SF}} \approx \sigma_z^{\text{SF}}$, there should be weak magnetic anisotropy between M_y and M_z in the paramagnetic tetragonal state. To probe the evolution of spin excitations in the paramagnetic orthorhombic ($T_N \leq T \leq T_s$) and tetragonal ($T > T_s$) phases, we study the temperature dependence of spin excitations at $E = 6$ meV from 2 to 80 K. Figures 4(c) and 4(d) show the raw data obtained for different neutron polarizations at the AF wave vectors $\mathbf{Q} = (1,0,0.5)$ and $(1,0,1.5)$, respectively, across the AF ordered, paramagnetic orthorhombic and tetragonal phases. In the low-temperature AF ordered state ($T = 2$ K), we find $\sigma_x^{\text{SF}} \approx \sigma_z^{\text{SF}}$ consistent with data in Fig. 3(a). On warming to the paramagnetic orthorhombic state [$T_N \leq T \leq T_s$, temperatures between the solid and dashed vertical lines in Figs. 4(c)–4(f)], we have $\sigma_x^{\text{SF}} > \sigma_z^{\text{SF}} > \sigma_y^{\text{SF}}$. This means anisotropic spin excitations at $\mathbf{Q} = (1,0,0.5)$ with $M_y - M_z = 0.14M_a + 0.86M_c - M_b > 0$ [Fig. 1(c)]. Finally, on warming to temperatures above T_s [Figs. 4(c) and 4(d)], spin excitations satisfy $\sigma_x^{\text{SF}} > \sigma_z^{\text{SF}} \approx \sigma_y^{\text{SF}}$ and are consistent with data in Figs. 4(a) and 4(b). Therefore, spin excitations in the paramagnetic tetragonal state of NaFeAs are more isotropic with $M_y - M_z = 0.14M_a + 0.86M_c - M_b \approx 0$.

Given the experimental evidence for anisotropic spin excitations in the paramagnetic orthorhombic phase of NaFeAs , it is important to determine its anisotropy along the crystallographic axes. In the AF ordered state, the low-energy spin waves from the two 90° rotated twin domains are centered around wave vectors $\mathbf{Q}_{\text{AF}} = (\pm 1, 0)$ and $(0, \pm 1)$, respectively, in reciprocal space. Therefore, low-energy spin waves from the $(\pm 1, 0)$ domain are not mixed with those from the $(0, \pm 1)$ domain. However, in the paramagnetic orthorhombic state, spin excitations at the wave vector $(\pm 1, 0)$ may be mixed with paramagnetic excitations from the domain associated with $(0, \pm 1)$, thus complicating the neutron polarization analysis. The key question is whether there is strong paramagnetic scattering at the wave vector $(0, \pm 1)$ in a completely detwinned sample associated with the AF wave vectors $(\pm 1, 0)$. Although such measurement for NaFeAs is unavailable, we note that neutron scattering experiments on a nearly 100% mechanically detwinned BaFe_2As_2 reveal that spin excitations in the paramagnetic tetragonal state are still centered mostly at $\mathbf{Q}_{\text{AF}} = (\pm 1, 0) \sim 20$ K above the AF and structural transition temperatures.⁴¹ Therefore, spin excitations of NaFeAs at the wave vectors $\mathbf{Q}_{\text{AF}} = (\pm 1, 0)$ may also have little contribution

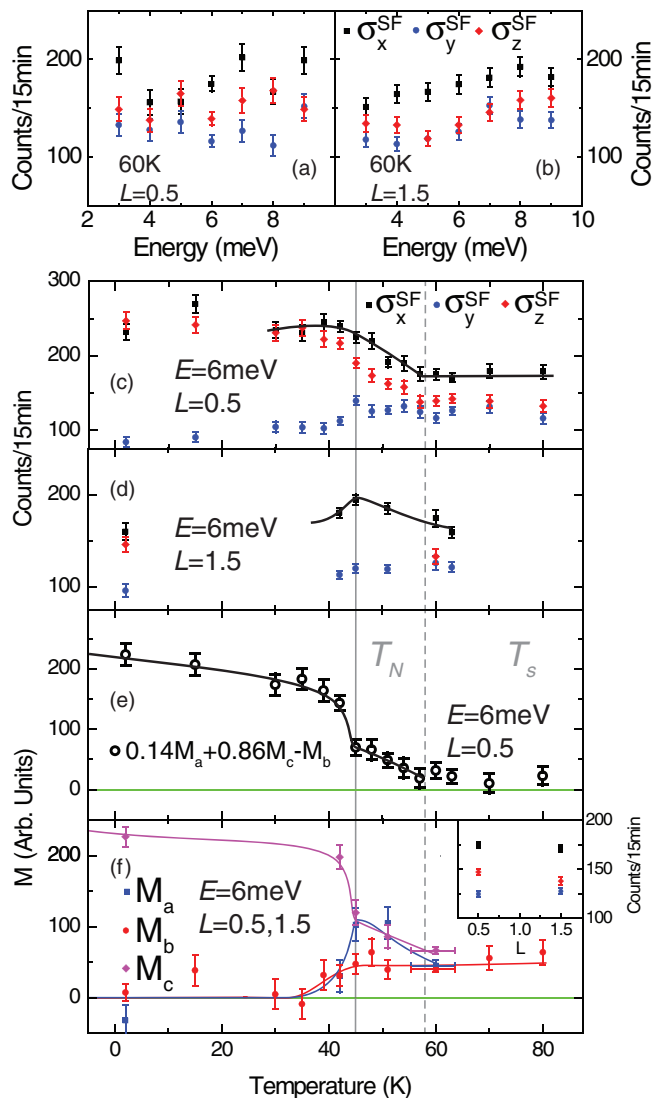


FIG. 4. (Color online) Constant- \mathbf{Q} scans at $T = 60$ K for $(1,0,0.5)$ and $(1,0,1.5)$ are shown in (a) and (b), respectively. Temperature dependence of the three spin-flip cross sections for the AF zone centers $(1,0,0.5)$ and $(1,0,1.5)$ are shown in (c) and (d). (e) The difference of the magnetic components M_y and M_z for $L = 0.5$ determined from σ_z^{SF} and σ_y^{SF} in (c). The temperature dependence of M_a , M_b , and M_c at the magnetic zone center are determined and plotted in (f). In cases where only cross sections for $L = 0.5$ are measured, only M_b can be determined, when σ_x^{SF} and σ_y^{SF} for $L = 1.5$ are in addition measured, all three components along crystal axes can be determined, when all three channels are measured for both $L = 0.5$ and $L = 1.5$, the overdetermination is used to improve estimates of M_a , M_b , and M_c . The point at $T \approx 60$ K is obtained by combining raw data from temperatures in the range indicated by horizontal bars and the constant- \mathbf{Q} scans in (a) and (b) from $E = 4$ – 8 meV, the combined σ_x^{SF} , σ_y^{SF} , and σ_z^{SF} for $L = 0.5$ and $L = 1.5$ are shown in the inset. The solid vertical gray line through (c), (d), (e), and (f) marks the magnetic transition temperature T_N , whereas the dashed gray line marks the structural transition temperature T_s . The solid lines in (e) and (f) are guides to the eye.

from those associated with the $(0, \pm 1)$ domain in the paramagnetic orthorhombic state. Assuming this is indeed the case, we can carry out neutron polarization analysis in the paramagnetic

orthorhombic phase similar to the AF ordered state. Figure 4(e) shows the temperature dependence of $0.14M_a + 0.86M_c - M_b$ for $\mathbf{Q} = (1,0,0.5)$ and $E = 6$ meV. The data show a clear kink at T_N and positive scattering below T_s , meaning $M_b < 0.14M_a + 0.86M_c$. The temperature dependence of M_a , M_b , and M_c shown in Fig. 4(f) are determined from combining the data in Figs. 4(a)–4(d). Inspection of the figure reveals clear in-plane magnetic anisotropy with $M_a > M_b$ in the paramagnetic orthorhombic phase that becomes much smaller in the paramagnetic tetragonal phase [Fig. 1(f)].

Our results suggest that whereas M_b , M_c evolve smoothly across T_N , M_a peaks around T_N indicating divergent longitudinally polarized critical magnetic fluctuations. Both σ_x^{SF} and unpolarized neutron scattering measures $M_y + M_z$, which is $0.14M_a + 0.86M_c + M_b$ for $\mathbf{Q} = (1,0,0.5)$ and $0.59M_a + 0.41M_c + M_b$ for $\mathbf{Q} = (1,0,1.5)$. If M_a dominates the critical fluctuations near T_N , one would expect a stronger peak due to critical fluctuations at $(1,0,1.5)$ than at $(1,0,0.5)$ since magnetic structural factor is larger at $(1,0,1.5)$.⁶ Comparison of our data measured at these two wave vectors [Figs. 4(c) and 4(d)] and unpolarized neutron scattering results in Ref. 37 suggest this is indeed the case. For a classical Heisenberg magnetic system with an Ising anisotropy term, one would expect diverging longitudinally polarized spin excitations at T_N consistent with our observation.³⁶

In previous polarized neutron measurements on parent compound BaFe_2As_2 ,³² it was found that the in-plane polarized spin waves exhibit a larger gap than the c -axis polarized ones. However, the spin anisotropy immediately disappears in the paramagnetic tetragonal state above T_N and T_s .³² In addition, while $\sigma_x^{\text{SF}} - \sigma_z^{\text{SF}} \propto M_b$ diverges at T_N , $\sigma_x^{\text{SF}} - \sigma_y^{\text{SF}} \propto (\sin^2 \theta M_a + \cos^2 \theta M_c)$ peaks at a temperature slightly below T_N .³² This is different from the results in Fig. 4. Since T_N and T_s occur at almost the same temperature in BaFe_2As_2 ,^{3,4} it is unclear whether the system also has magnetic anisotropy in the paramagnetic orthorhombic phase. The discovery of an in-plane spin excitation anisotropy in the paramagnetic orthorhombic phase of NaFeAs suggests the presence of a strong spin-orbit coupling in such a state.^{31,34,42–44} However, we cannot distinguish if such anisotropy is a sole manifestation of spin nematicity or a consequence of the orbital ordering.^{22–26} In a recent x-ray diffraction experiment under pulsed magnetic fields, in-plane field-induced static susceptibility anisotropy with $\chi_b > \chi_a$ in the AF ordered state is found to extend to the paramagnetic orthorhombic phase of electron-underdoped $\text{Ba}(\text{Fe}_{1-x}\text{Co}_x)_2\text{As}_2$.²⁸ This is 90° rotated from the in-plane dynamic susceptibility anisotropy ($M_a > M_b$ or $\chi_a'' > \chi_b''$) in the paramagnetic orthorhombic state of NaFeAs. While the static susceptibility anisotropy remains unchanged from the AF ordered phase to the paramagnetic orthorhombic phase in $\text{Ba}(\text{Fe}_{1-x}\text{Co}_x)_2\text{As}_2$,²⁸ there is a dramatic switch over of the spin excitation anisotropy across T_N in NaFeAs, changing from the entirely c -axis polarized spin waves ($M_c \gg M_a \approx M_b \approx 0$) in the AF ordered phase to $M_a \geq M_c > M_b$ in the paramagnetic orthorhombic state. Finally, the spin anisotropy becomes much smaller in the paramagnetic tetragonal phase. We note that the static in-plane susceptibility anisotropy observed in transport²⁷ and x-ray diffraction experiments²⁸ occurs at the zero wave vector, while the dynamic susceptibility anisotropy in NaFeAs is at the AF wave vectors $\mathbf{Q}_{\text{AF}} = (\pm 1, 0)$.

III. DISCUSSION AND CONCLUSIONS

To qualitatively understand these results, we note that the orthorhombic lattice distortion below T_s lifts the degeneracy between Fe d_{xz} and d_{yz} orbitals and leads to a ferro-orbital order with more doubly occupied Fe d_{xz} orbitals and more singly occupied Fe d_{yz} orbitals.²² In the case of NaFeAs, the Fermi surfaces evolve dramatically from the paramagnetic tetragonal state to the AF ordered state and the splitting of the d_{xz} and d_{yz} orbitals starts to occur at a temperature above T_s .¹² The angular momentum of d_{yz} orbitals lies along the a -axis direction, which pins the ordering spin moment along the a axis via spin-orbit interaction. This is indeed observed experimentally as shown in Fig. 1(a).³ Although the electronic structure undergoes an orbital-dependent reconstruction in the nematic state above T_s , primarily involving the splitting of d_{xz} - and d_{yz} -dominated bands, the splitting mostly occurs in the temperature range above T_N , and there are only small changes across T_N .¹² This is different from the temperature dependent spin dynamic susceptibility across T_N [Fig. 1(f)], but consistent with the notion that ferro-orbital ordering involving d_{xz} and d_{yz} bands plays a minor role.¹² Therefore, it is more likely that the observed dynamic susceptibility anisotropy is a manifestation of dynamic spin nematicity coupled with orbital ordering. For a typical second order AF phase transition, critical spin fluctuations should exhibit a peak at T_N .⁴⁵ From Fig. 4(f) we see that spin excitations in NaFeAs are dominated by the longitudinal fluctuations (M_a or χ_a'') near T_N , consistent with diverging longitudinally polarized spin excitations in a Heisenberg antiferromagnet with Ising spin anisotropy.³⁶ Given the small lattice distortion in the paramagnetic orthorhombic phase of NaFeAs,⁷ it is unlikely such an anisotropy term could arise from the lattice distortion. This is consistent with the fact that similar in-plane spin excitation anisotropy has also been observed in the paramagnetic tetragonal phase of superconducting $\text{BaFe}_{1.904}\text{Ni}_{0.096}\text{As}_2$.³⁵ Instead, the observed in-plane spin excitation anisotropy is more likely to arise from orbital ordering or anisotropic exchange interactions due to spin nematicity.

In summary, we have discovered that low-energy spin waves in NaFeAs are entirely c -axis polarized for energies below ~ 10 meV. On warming the system across T_N to the paramagnetic orthorhombic state, a clear in-plane anisotropy develops in the low-energy spin excitations spectra, resulting in $M_a \geq M_c > M_b$. Finally, spin excitations become more isotropic in the paramagnetic tetragonal phase above T_s . These results indicate that the spin excitation anisotropy in superconducting iron pnictides originates from similar anisotropy already present in their parent compounds, and suggest the presence of a spin nematic phase in the paramagnetic orthorhombic state of NaFeAs.

ACKNOWLEDGMENTS

We thank Haifeng Li and T. Netherton for experimental assistance, and Jiangping Hu and Fa Wang for helpful discussions. The single crystal growth efforts and neutron scattering work at UTK and Rice are supported by the US DOE, BES, through Contract DE-FG02-05ER46202. Work at IOP is supported by MOST (973 Project: 2012CB82400). The work at the HFIR, ORNL, was sponsored by the Scientific User Facilities Division, BES, US DOE.

*pdai@rice.edu

- ¹Y. Kamihara, T. Watanabe, M. Hirano, and H. Hosono, *J. Am. Chem. Soc.* **130**, 3296 (2008).
- ²C. de la Cruz, Q. Huang, J. W. Lynn, J. Y. Li, W. Ratcliff II, J. L. Zarestky, H. A. Mook, G. F. Chen, J. L. Luo, N. L. Wang, and P. C. Dai, *Nature (London)* **453**, 899 (2008).
- ³Q. Huang, Y. Qiu, W. Bao, M. A. Green, J. W. Lynn, Y. C. Gasparovic, T. Wu, G. Wu, and X. H. Chen, *Phys. Rev. Lett.* **101**, 257003 (2008).
- ⁴M. G. Kim, R. M. Fernandes, A. Kreyssig, J. W. Kim, A. Thaler, S. L. Bud'ko, P. C. Canfield, R. J. McQueeney, J. Schmalian, and A. I. Goldman, *Phys. Rev. B* **83**, 134522 (2011).
- ⁵C. W. Chu, F. Chen, M. Gooch, A. M. Guloy, B. Lorenz, B. Lv, K. Sasmal, Z. J. Tang, J. H. Tapp, and Y. Y. Xue, *Physica C* **469**, 326 (2009).
- ⁶S. L. Li, C. de la Cruz, Q. Huang, G. F. Chen, T.-L. Xia, J. L. Luo, N. L. Wang, and P. C. Dai, *Phys. Rev. B* **80**, 020504(R) (2009).
- ⁷Y. Song, S. V. Carr, X. Lu, C. Zhang, Z. C. Sims, N. F. Luttrell, S. Chi, Y. Zhao, J. W. Lynn, and P. C. Dai, *Phys. Rev. B* **87**, 184511 (2013).
- ⁸P. C. Dai, J. P. Hu, and E. Dagotto, *Nat. Phys.* **8**, 709 (2012).
- ⁹I. R. Fisher, L. Degiorgi, and Z. X. Shen, *Rep. Prog. Phys.* **74**, 124506 (2011).
- ¹⁰R. M. Fernandes, L. H. VanBebber, S. Bhattacharya, P. Chandra, V. Keppens, D. Mandrus, M. A. McGuire, B. C. Sales, A. S. Sefat, and J. Schmalian, *Phys. Rev. Lett.* **105**, 157003 (2010).
- ¹¹M. Yi, D. H. Lu, J.-H. Chu, J. G. Analytis, A. P. Sorini, A. F. Kemper, B. Moritz, S.-K. Mo, R. G. Moore, M. Hashimoto, W. S. Lee, Z. Hussain, T. P. Devereaux, I. R. Fisher, and Z.-X. Shen, *Proc. Natl. Acad. Sci. USA* **108**, 6878 (2011).
- ¹²Y. Zhang, C. He, Z. R. Ye, J. Jiang, F. Chen, M. Xu, Q. Q. Ge, B. P. Xie, J. Wei, M. Aeschlimann, X. Y. Cui, M. Shi, J. P. Hu, and D. L. Feng, *Phys. Rev. B* **85**, 085121 (2012).
- ¹³M. Yi, D. H. Lu, R. G. Moore, K. Kihou, C.-H. Lee, A. Iyo, H. Eisaki, T. Yoshida, A. Fujimori, and Z.-X. Shen, *New J. Phys.* **14**, 073019 (2012).
- ¹⁴L. W. Harriger, H. Q. Luo, M. S. Liu, C. Frost, J. P. Hu, M. R. Norman, and P. C. Dai, *Phys. Rev. B* **84**, 054544 (2011).
- ¹⁵S. Kasahara, H. J. Shi, K. Hashimoto, S. Tonegawa, Y. Mizukami, T. Shibauchi, K. Sugimoto, T. Fukuda, T. Terashima, Andriy H. Nevidomskyy, and Y. Matsuda, *Nature (London)* **486**, 382 (2012).
- ¹⁶T.-M. Chuang, M. P. Allan, J. Lee, Y. Xie, Ni Ni, S. L. Bud'ko, G. S. Boebinger, P. C. Canfield, and J. C. Davis, *Science* **327**, 181 (2010).
- ¹⁷M. P. Allan, T.-M. Chuang, F. Massee, Yang Xie, Ni Ni, S. L. Bud'ko, G. S. Boebinger, Q. Wang, D. S. Dessau, P. C. Canfield, M. S. Golden, and J. C. Davis, *Nat. Phys.* **9**, 220 (2013).
- ¹⁸E. P. Rosenthal, E. F. Andrade, C. J. Arguello, R. M. Fernandes, L. Y. Xing, X. C. Wang, C. Q. Jin, A. J. Millis, and A. N. Pasupathy, arXiv:1307.3526.
- ¹⁹E. Fradkin, S. A. Kivelson, M. J. Lawler, J. P. Eisenstein, and A. P. Mackenzie, *Annu. Rev. Condens. Matter Phys.* **1**, 153 (2010).
- ²⁰J. P. Hu and C. K. Xu, *Physica C* **481**, 215 (2012).
- ²¹R. M. Fernandes, A. V. Chubukov, J. Knolle, I. Eremin, and J. Schmalian, *Phys. Rev. B* **85**, 024534 (2012).
- ²²C. C. Lee, W. G. Yin, and W. Ku, *Phys. Rev. Lett.* **103**, 267001 (2009).
- ²³F. Krüger, S. Kumar, J. Zaanen, and J. van den Brink, *Phys. Rev. B* **79**, 054504 (2009).
- ²⁴W. C. Lv, J. S. Wu, and P. Phillips, *Phys. Rev. B* **80**, 224506 (2009).
- ²⁵C.-C. Chen, J. Maciejko, A. P. Sorini, B. Moritz, R. R. P. Singh, and T. P. Devereaux, *Phys. Rev. B* **82**, 100504(R) (2010).
- ²⁶B. Valenzuela, E. Bascones, and M. J. Calderón, *Phys. Rev. Lett.* **105**, 207202 (2010).
- ²⁷J.-H. Chu, J. G. Analytis, D. Press, K. De Greve, T. D. Ladd, Y. Yamamoto, and I. R. Fisher, *Phys. Rev. B* **81**, 214502 (2010).
- ²⁸J. P. C. Ruff, J.-H. Chu, H.-H. Kuo, R. K. Das, H. Nojiri, I. R. Fisher, and Z. Islam, *Phys. Rev. Lett.* **109**, 027004 (2012).
- ²⁹M. Nakajima, S. Ishida, Y. Tomioka, K. Kihou, C. H. Lee, A. Iyo, T. Ito, T. Kakeshita, H. Eisaki, and S. Uchida, *Phys. Rev. Lett.* **109**, 217003 (2012).
- ³⁰S. Ishida, M. Nakajima, T. Liang, K. Kihou, C. H. Lee, A. Iyo, H. Eisaki, T. Kakeshita, Y. Tomioka, T. Ito, and S. Uchida, *Phys. Rev. Lett.* **110**, 207001 (2013).
- ³¹O. J. Lipscombe, L. W. Harriger, P. G. Freeman, M. Enderle, C. L. Zhang, M. Y. Wang, T. Egami, J. P. Hu, T. Xiang, M. R. Norman, and P. C. Dai, *Phys. Rev. B* **82**, 064515 (2010).
- ³²N. Qureshi, P. Steffens, S. Wurmehl, S. Aswartham, B. Büchner, and M. Braden, *Phys. Rev. B* **86**, 060410(R) (2012).
- ³³M. Liu, C. Lester, J. Kulda, X. Lu, H. Luo, M. Wang, S. M. Hayden, and P. C. Dai, *Phys. Rev. B* **85**, 214516 (2012).
- ³⁴C. L. Zhang, M. S. Liu, Y. X. Su, L.-P. Regnault, M. Wang, G. T. Tan, Th. Brückel, T. Egami, and P. C. Dai, *Phys. Rev. B* **87**, 081101(R) (2013).
- ³⁵H. Luo, M. Wang, C. Zhang, X. Lu, L.-P. Regnault, R. Zhang, S. Li, J. Hu, and P. C. Dai, *Phys. Rev. Lett.* **111**, 107006 (2013).
- ³⁶M. F. Collin, *Magnetic Critical Scattering* (Oxford University Press, New York, 1989), Chap. 8.
- ³⁷J. T. Park, G. Friemel, T. Loew, V. Hinkov, Y. Li, B. H. Min, D. L. Sun, A. Ivanov, A. Piovano, C. T. Lin, B. Keimer, Y. S. Kwon, and D. S. Inosov, *Phys. Rev. B* **86**, 024437 (2012).
- ³⁸K. Matan, R. Morinaga, K. Iida, and T. J. Sato, *Phys. Rev. B* **79**, 054526 (2009).
- ³⁹Using time-of-flight neutron spectroscopy, we have collected spin wave data on NaFeAs throughout the entire Brillouin in the AF ordered state. Based on Heisenberg Hamiltonian fits to the high-energy spin waves, we determine effective magnetic exchange couplings along different crystallographic directions.
- ⁴⁰C. Wang, R. Zhang, F. Wang, H. Luo, L. P. Regnault, P. C. Dai, and Y. Li, arXiv:1309.7553.
- ⁴¹X. Y. Lu, J. T. Park, R. Zhang, H. Q. Luo, A. H. Nevidomskyy, Q. Si, and P. C. Dai (unpublished).
- ⁴²P. Babkevich, B. Roessli, S. N. Gvasaliya, L.-P. Regnault, P. G. Freeman, E. Pomjakushina, K. Conder, and A. T. Boothroyd, *Phys. Rev. B* **83**, 180506(R) (2011).
- ⁴³K. Prokeš, A. Hiess, W. Bao, E. Wheeler, S. Landsgesell, and D. N. Argyriou, *Phys. Rev. B* **86**, 064503 (2012).
- ⁴⁴P. Steffens, C. H. Lee, N. Qureshi, K. Kihou, A. Iyo, H. Eisaki, and M. Braden, *Phys. Rev. Lett.* **110**, 137001 (2013).
- ⁴⁵L. W. Harriger, A. Schneidewind, S. L. Li, J. Zhao, Z. C. Li, W. Lu, X. L. Dong, F. Zhou, Z. X. Zhao, J. P. Hu, and P. C. Dai, *Phys. Rev. Lett.* **103**, 087005 (2009).